Observing methane emissions from space with the next generation of satellite instruments: from global OH monitoring down to individual point sources

Daniel Jacob
with Yuzhong Zhang, Bram Maasakkers, Daniel Varon

HARVARD UNIVERSITY
ATMOSPHERIC CHEMISTRY MODELING GROUP

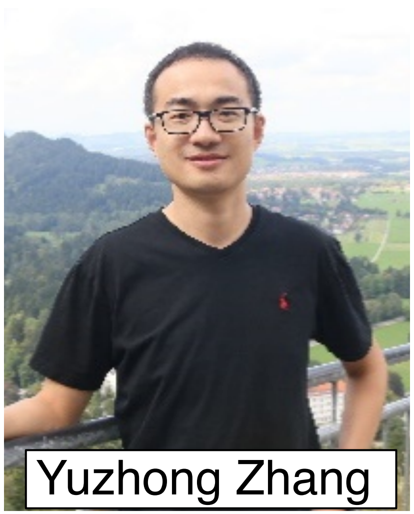

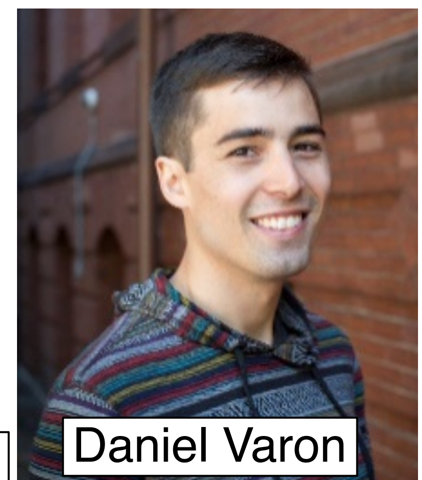

Supported by NASA, EDF, and GHGSat, Inc.

Global OH monitoring has relied on the methylchloroform proxy

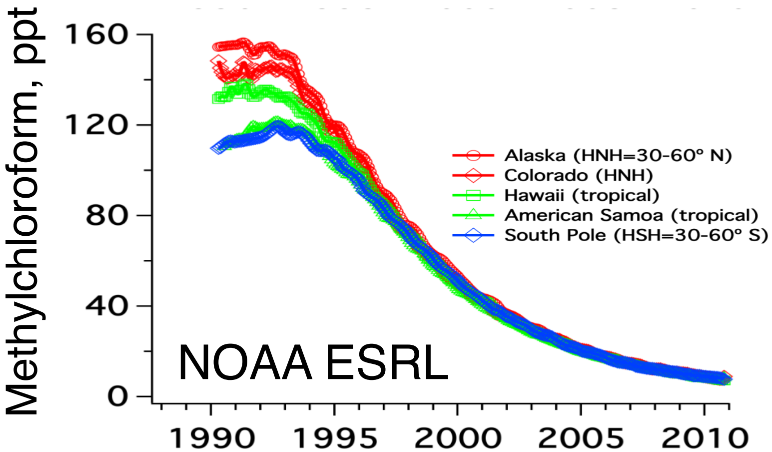

Mass balance for methylchloroform:

$$\frac{dm_{MCF}}{dt} = -k\overline{[\mathrm{OH}]}\, m_{MCF} + \text{minor terms}$$

But errors on this proxy are large and growing, and assessing OH trends is highly uncertain

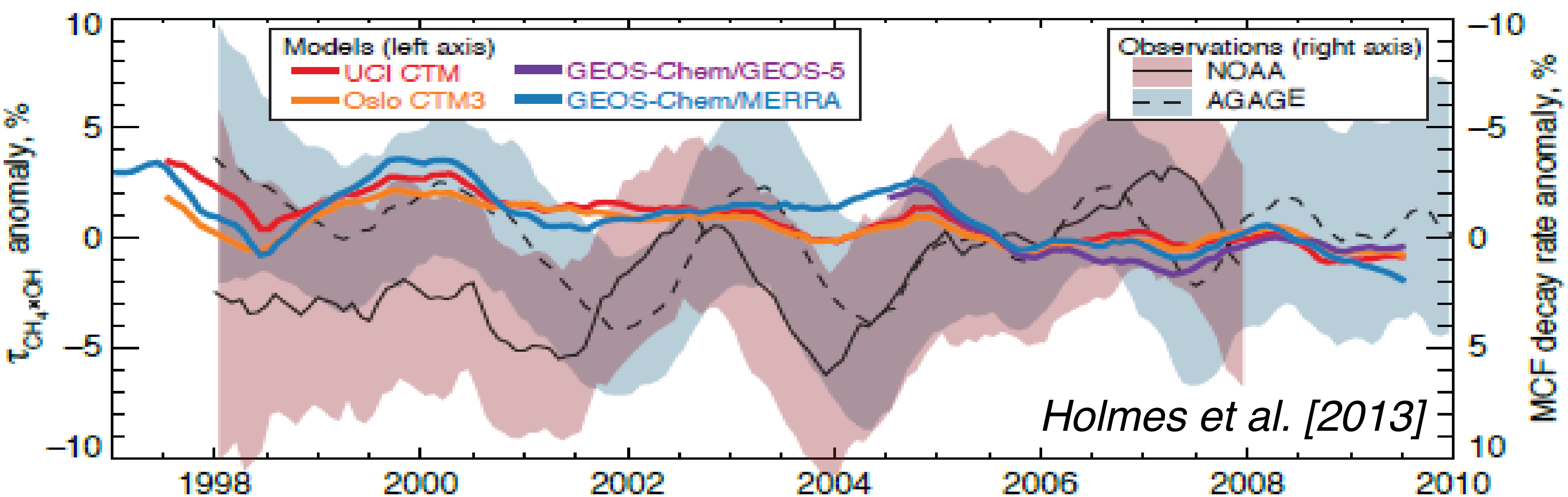

Use methane as a proxy instead: $$\frac{dm_{CH4}}{dt} = E - k\overline{[\mathrm{OH}]}\, m_{CH4} + \text{minor terms}$$

Optimize with methane observations from space

Distribution of tropospheric methane + OH loss rate (GEOS-Chem model)

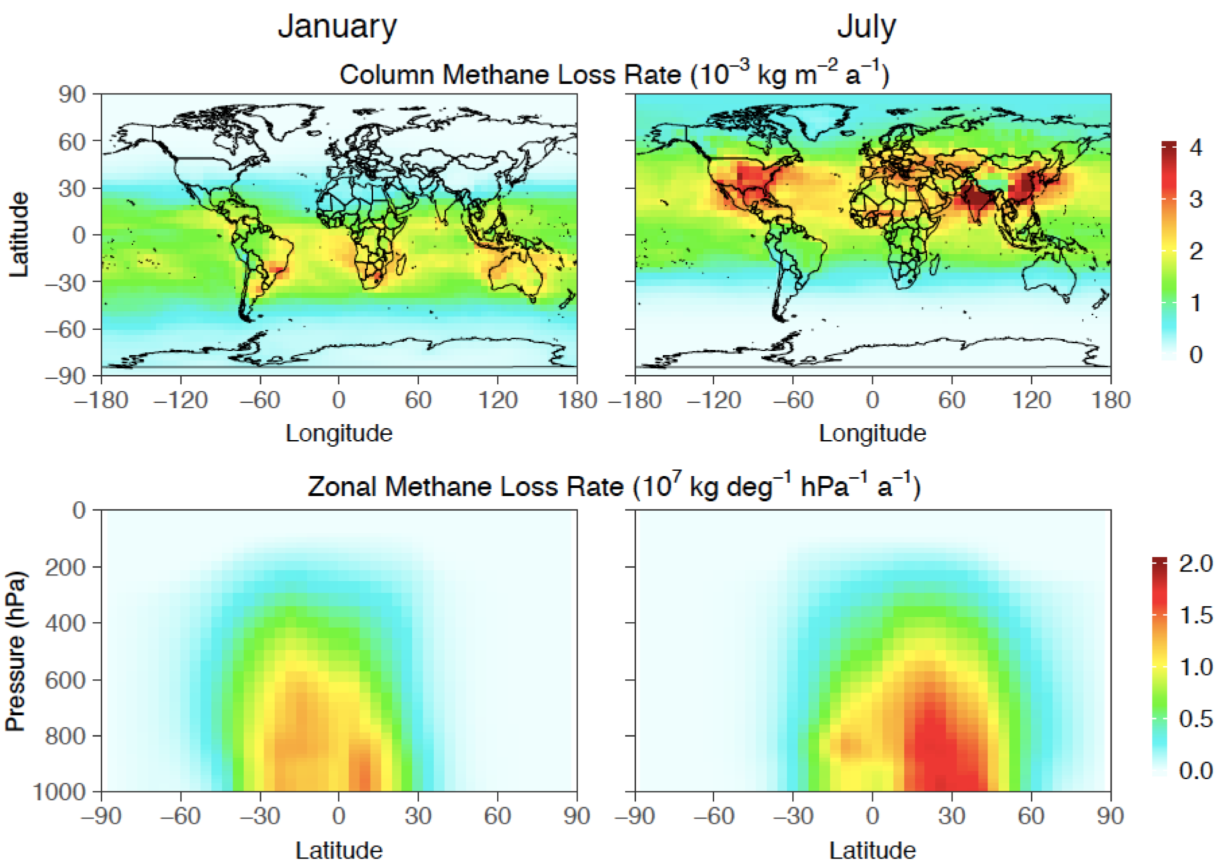

SWIR and TIR satellite observations

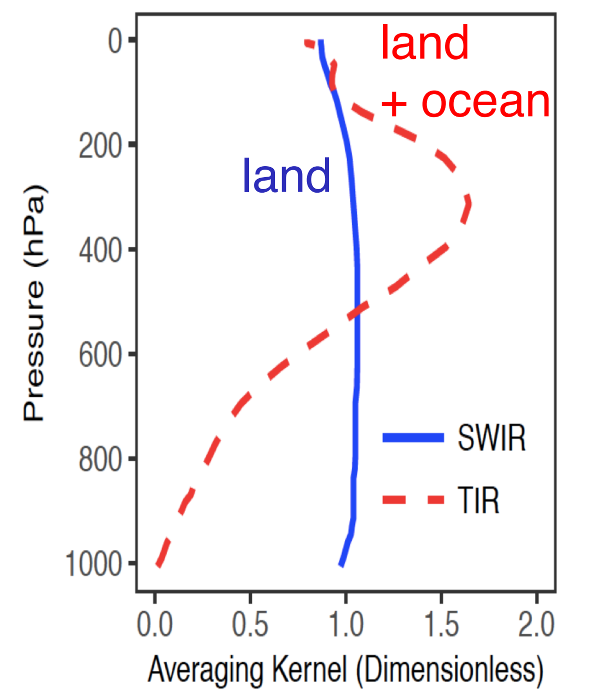

Loss pattern has broad meridional and seasonal signatures, distinct from emission signatures in inversions of methane satellite data

Zhang et al. [2018]

Inversion of 2010-2015 GOSAT methane data shows promise

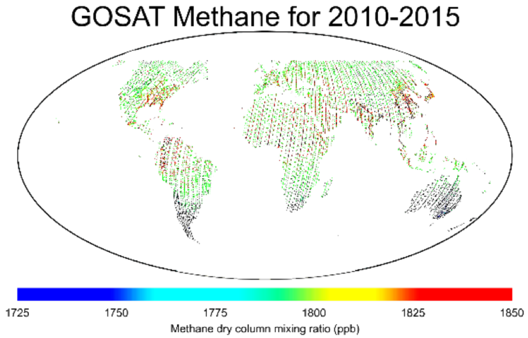

Analytical inversion using GEOS-Chem forward model with joint Bayesian optimization of

- methane emissions (4°x5°)
- 2010-2015 trends (4°x5°)
- annual global OH concentration

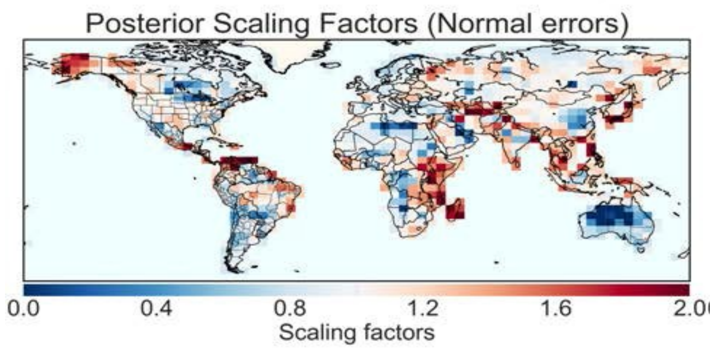

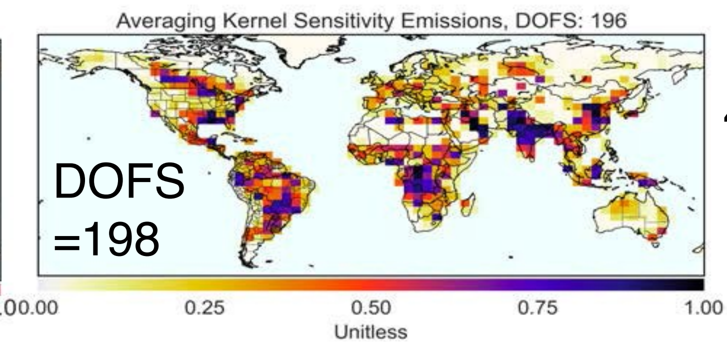

4°x5° correction to EDGAR+WetCHARTs inventories

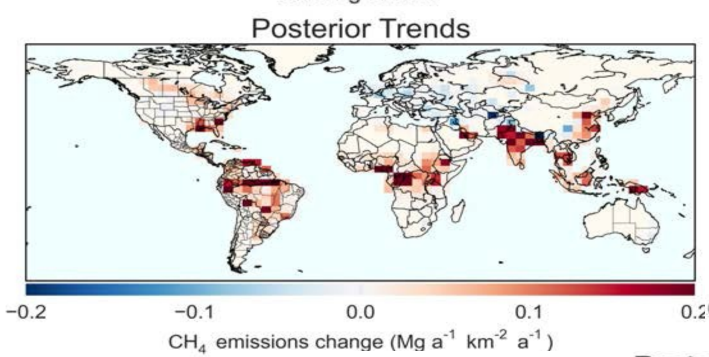

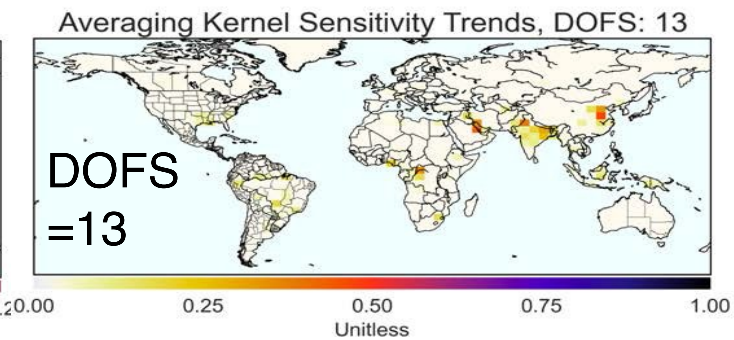

Emission trends: tropical increases

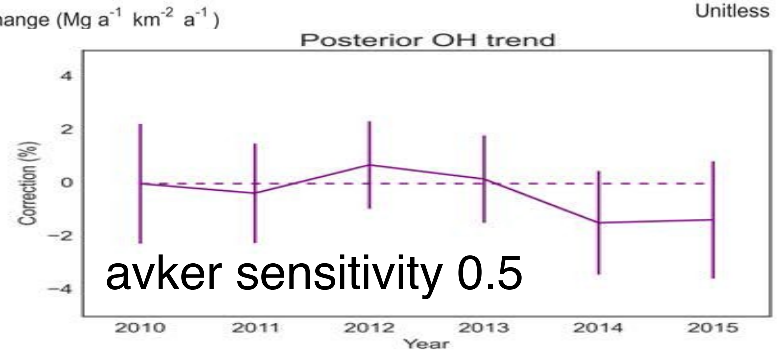

OH trend: -2% contributes to methane increase

Maasakkers et al. [2018]

What can we achieve with the next generation of satellite instruments?

Conduct OSSE to assess potential for using methane from space as proxy for global OH

- SWIR: TROPOMI, global daily, 3% success rate, 0.6% precision
- TIR: AIRS/CrIS, global 2x/day, 60% success rate, 2% precision

12 different OH distributions (ACCMIP ensemble)

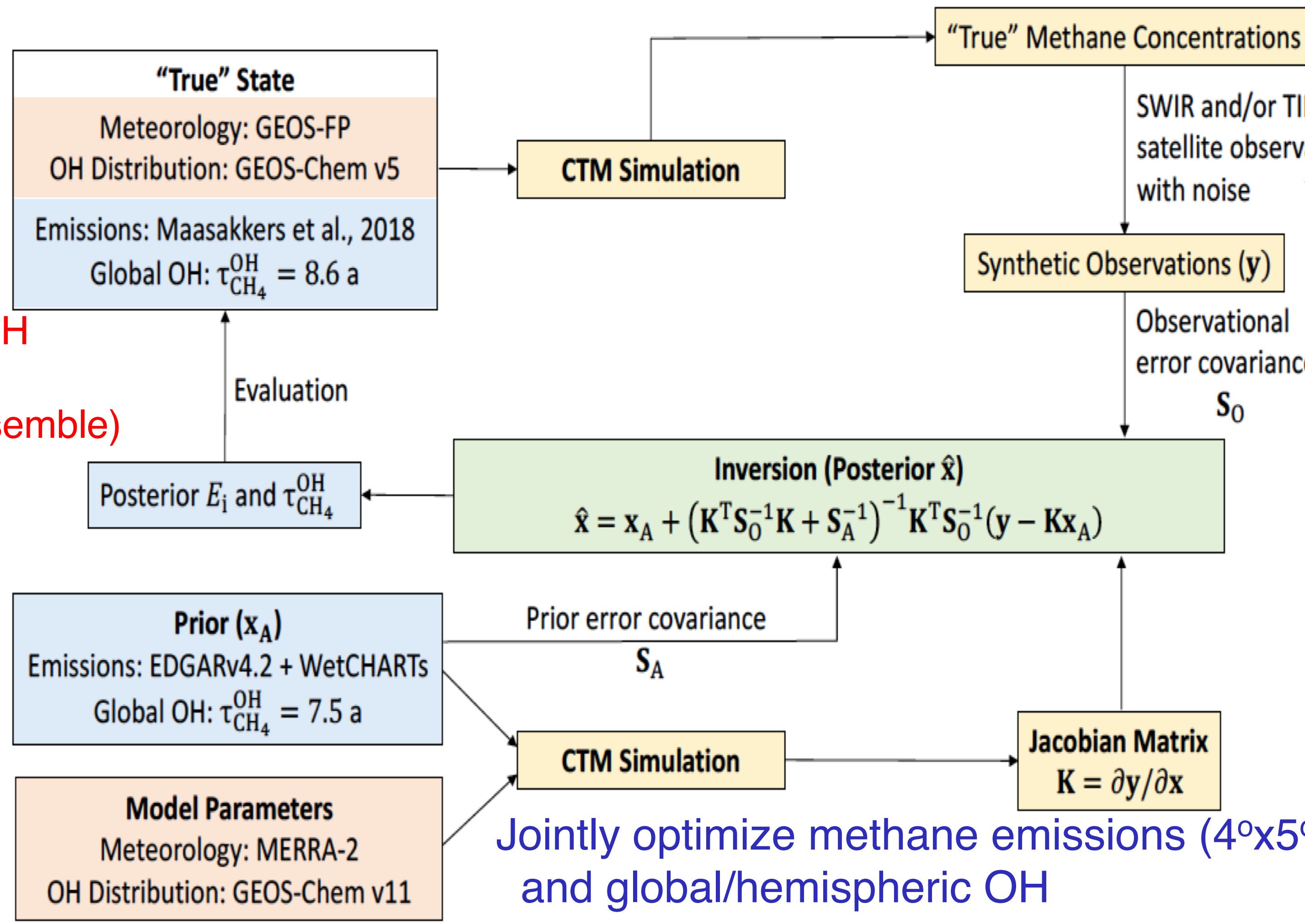

Jointly optimize methane emissions (4°x5° grid) and global/hemispheric OH

Zhang et al. [2018]

Ability of satellite methane data to constrain OH and its trend

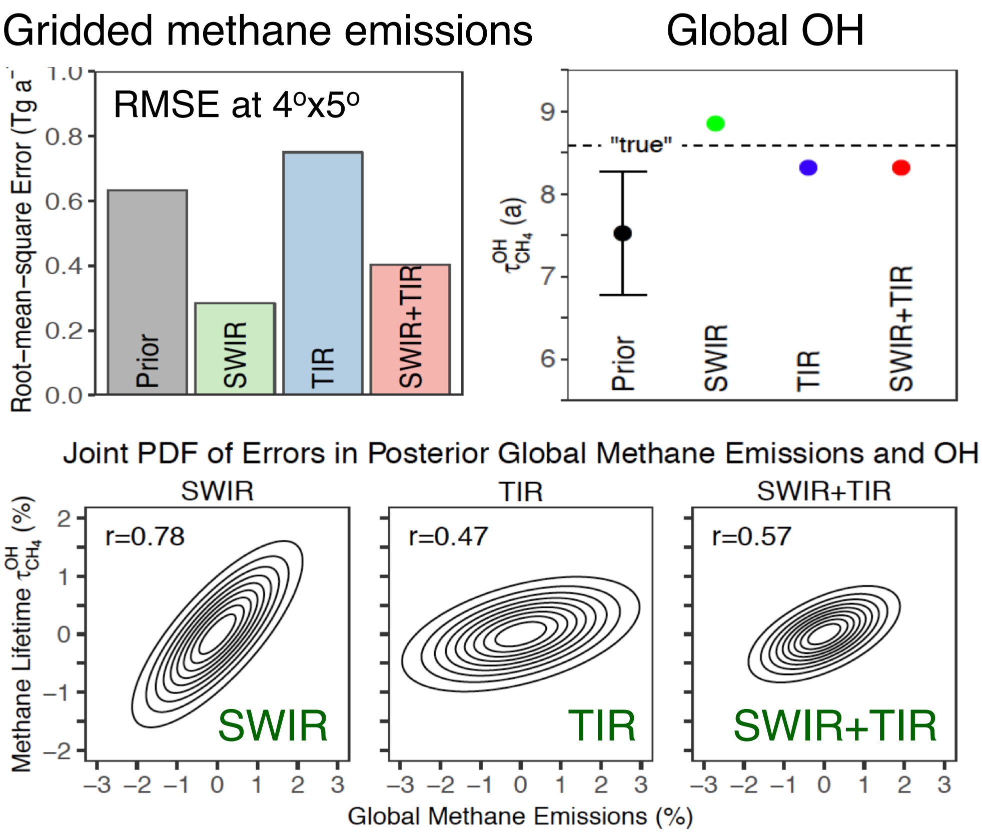

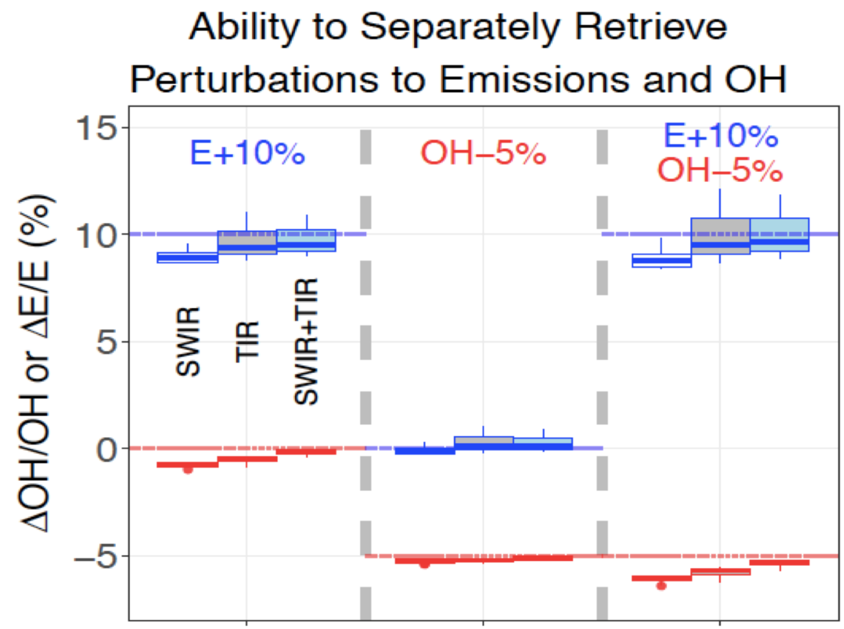

- SWIR is essential for retrieving global distribution of emissions
- TIR enables better separation of global emissions and OH
- Global emissions and OH concentrations, and their trend, can be separately retrieved

Zhang et al. [2018]

Retrieving point source emission rates from high-resolution remote sensing of instantaneous methane plumes

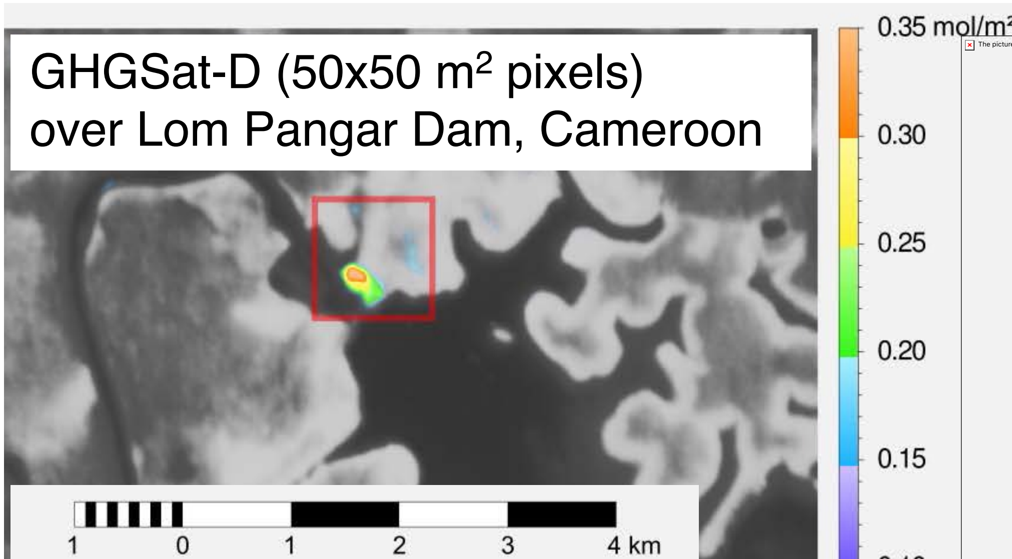

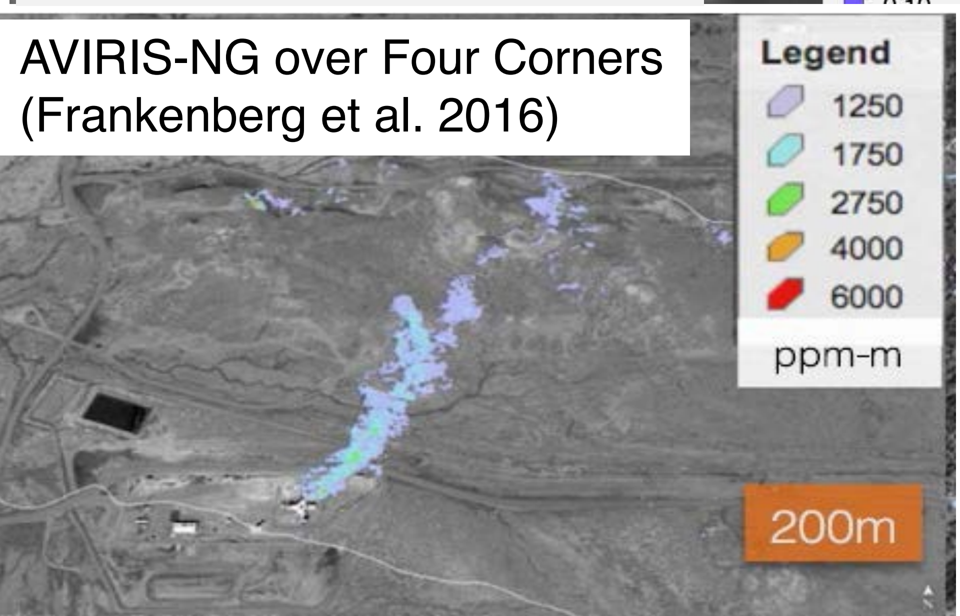

WRF large-eddy simulation at 50x50 m² resolution

Varon et al. [2018]

Methods for inferring point source rates Q from instantaneous observation of column plume enhancements $\Delta\Omega$

1. Gaussian plume inversion

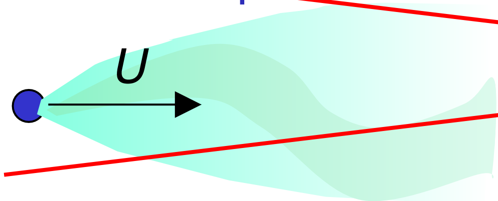

$$Q = U\Delta\Omega(x,y)\sqrt{2\pi}\sigma_y(x)e^{\frac{y^2}{2\sigma_y(x)^2}}$$

Fails for plumes < 10 km due to non-Gaussian behavior

2. Source pixel mass balance

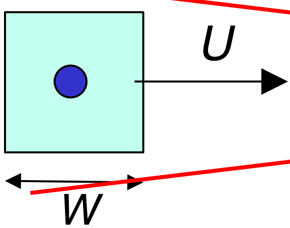

$$Q = \frac{UWp}{g\Omega_a}\Delta\Omega$$

Fails for pixels < 1 km because eddy flow dominates ventilation

3. Cross-sectional flux

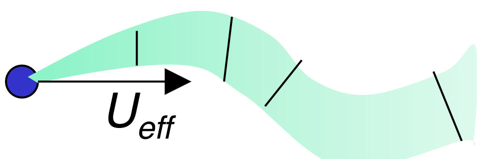

$$Q = U_{eff}\overline{\int_{plume\ width}\Delta\Omega(x,y)dy}$$

Both methods require estimates of plume size L and effective wind speed U_{eff}

4. Integrated mass enhancement (IME)

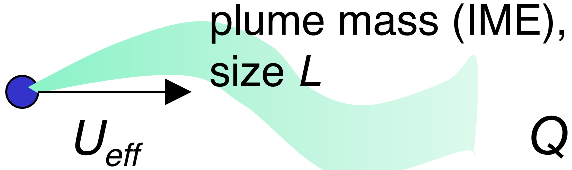

$$Q = \frac{1}{\tau}\iint_{plume\ area}\Delta\Omega(x,y)dxdy = \frac{U_{eff}}{L}\iint_{plume\ area}\Delta\Omega(x,y)dxdy$$

Define plume size *L for c*ross-sectional flux and IME methods

Pattern recognition algorithm excluding pixels with signal/noise <1

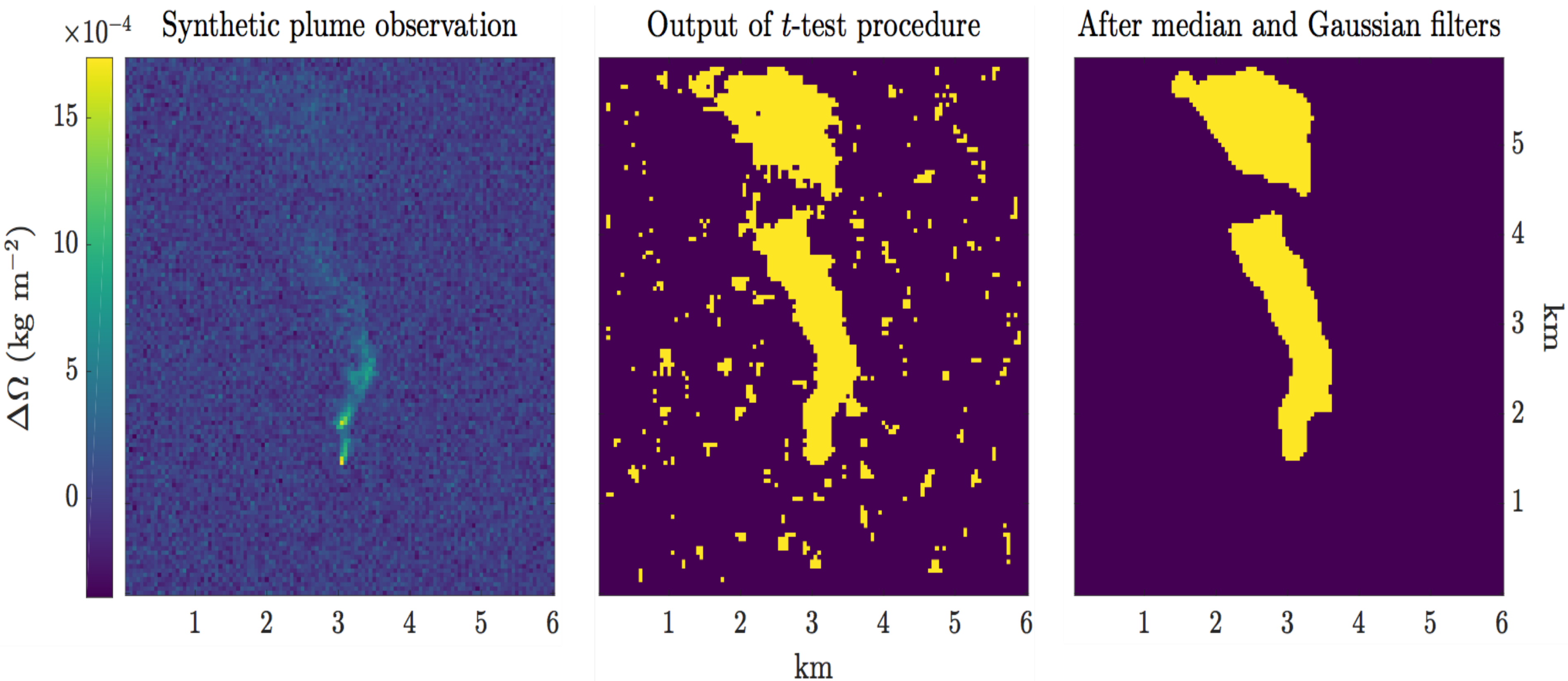

- Axis of plume defines wind direction for cross-sectional flux method;
- Area *A* of plume defines plume size $L = \sqrt{A}$ for IME method

Varon et al. [2018]

Relating effective wind speed to the local 10-m wind speed

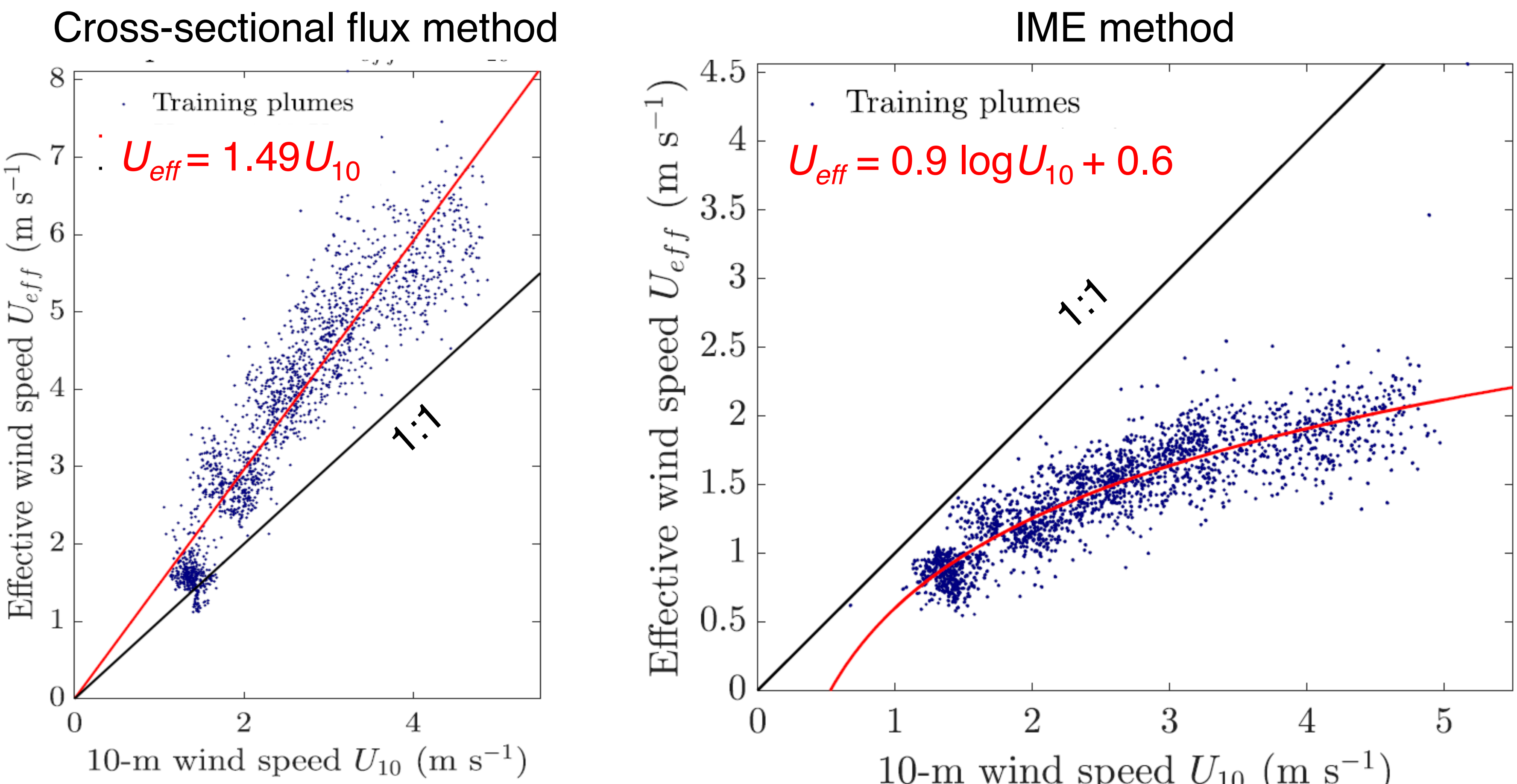

In IME method, the plume observations contain some info on wind speed; makes method less sensitive to wind speed error

Varon et al. [2018]

What to do in absence of local wind speed data?

Get estimate from operational meteorological data base, but incur representation error

Illustrate with comparison of global GEOS-FP data to 5-min US airport data

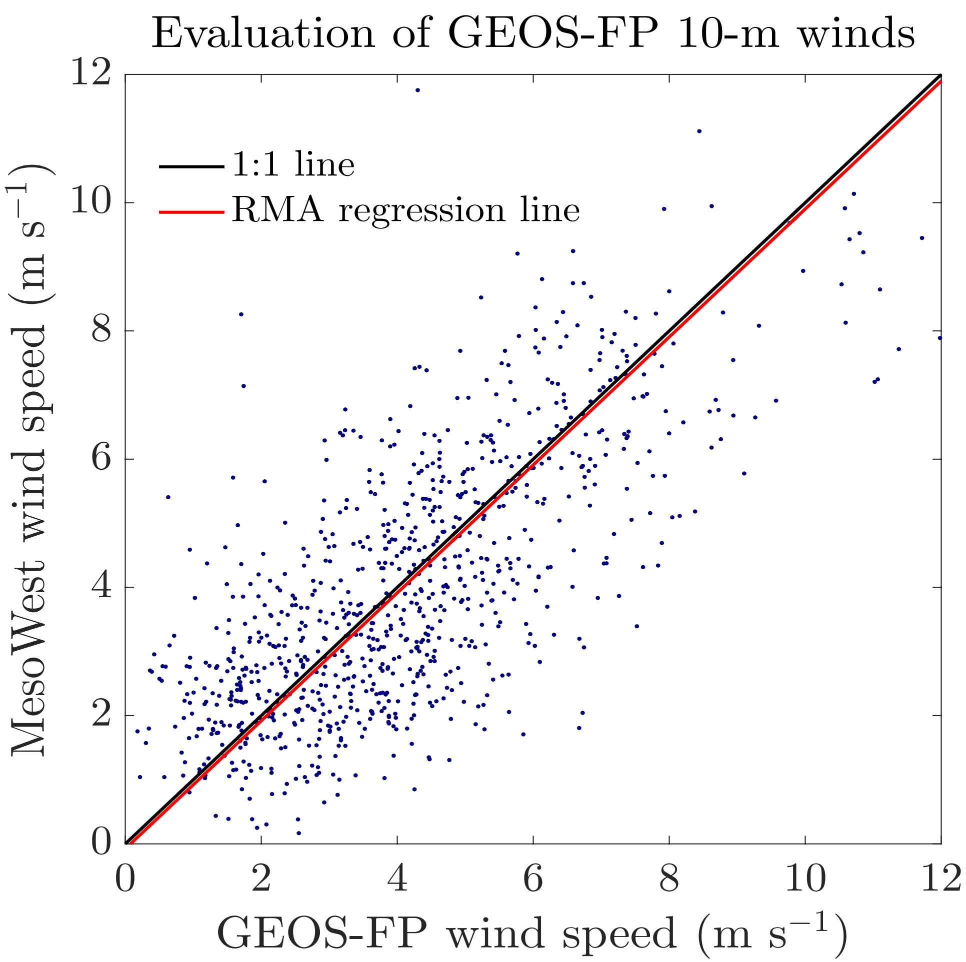

Error standard deviation:
2 m s^{-1} for 5-min averaging time
1..3 m s^{-1} for 1-h averaging time

Low wind speeds have large relative error

Varon et al. [2018]

Testing the methods with independent set of LES plumes

Ability to retrieve "true" source rate *Q*

IME method

x-sectional flux method

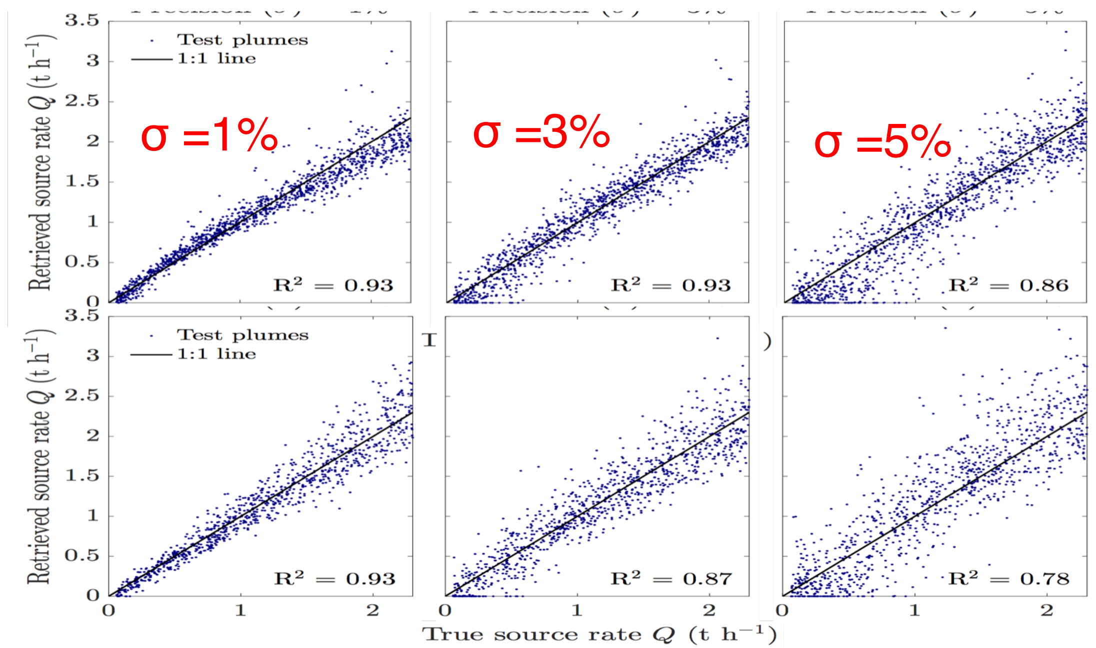

Summary of GHGSat precision in retrieving point source rates *Q* (50x50 m^2 pixels)

Method	Instrument precision			If no local wind data
	1%	3%	5%	
IME	0.07 t h^{-1} + 5%	0.13 t h^{-1} + 7%	0.17 t h^{-1} + 12%	15-50%
x-sectional flux	0.07 t h^{-1} + 8%	0.18 t h^{-1} + 8%	0.26 t h^{-1} + 12%	30-65%

7→ 2 m s^{-1}

- IME method better than x-sectional flux method
- Sources > 0.5 t h^{-1} (75% of US GHGRP) can be usefully retrieved
- Lack of local wind data can dominate error at low winds

Varon et al. [2018]

Precision of the methods for retrieving point source rates

GHGSat observations for 50x50 m^2 pixels with 1-5% instrument precision

Method	Instrument precision			If no local wind data
	1%	3%	5%	
IME	0.07 t h^{-1} + 5%	0.13 t h^{-1} + 7%	0.17 t h^{-1} + 12%	15-50%
x-sectional flux	0.07 t h^{-1} + 8%	0.18 t h^{-1} + 8%	0.26 t h^{-1} + 12%	30-65%

- Absolute precision allows detection of sources greater than 0.5 t h^{-1} (4 kt $year^{-1}$), which contribute more than 75% of US GHGRP sources
- Low winds are good for source detection but not for source quantification
- IME method is better than x-sectional flux method, esp. in absence of local wind data

Next steps:

- Include inhomogeneous noise in the OSSE
- Work with GHGSat airborne simulator, other aircraft observations

Varon et al. [2018]

Assessing the effect of errors in global OH distribution

OSSEs with 12 different "true" OH distributions from ACCMIP ensemble

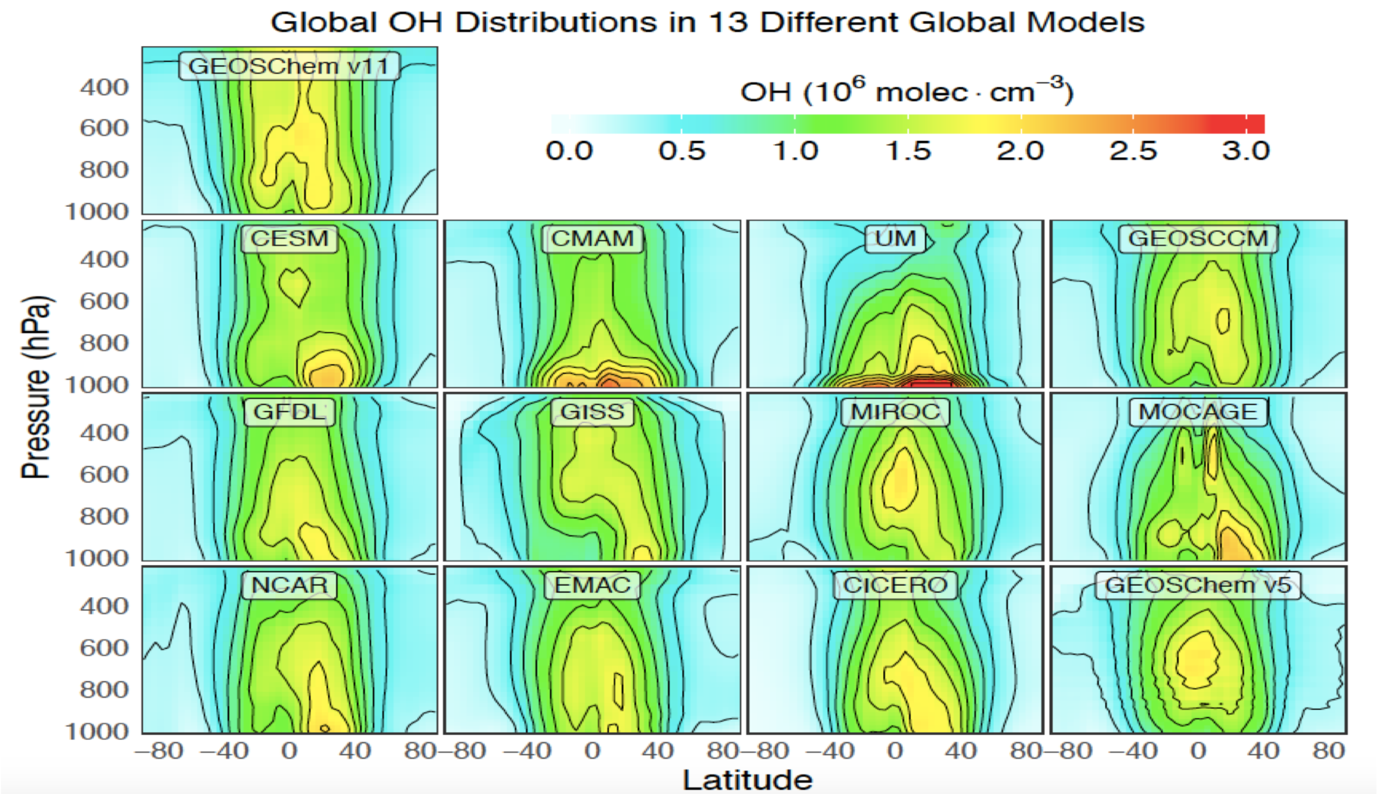

- Error in OH distribution can cause 3-7% systematic error in retrieving global OH, but error on retrieving OH trends is much less (previous slide)

Zhang et al. [2018]